

Basal-plane anisotropy of field-induced multipolar order in tetragonal CeRh_2As_2

K. Semeniuk,^{1,*} B. Schmidt,¹ C. Marcenat,² M. Pfeiffer,³ A. Demuer,⁴ L. Behera,³ T. Klein,⁵ S. Khim,¹ and E. Hassinger^{6,1,*}

¹Max Planck Institute for Chemical Physics of Solids, 01187 Dresden, Germany

²Université Grenoble Alpes, CEA, Grenoble-INP, IRIG, Phelip, 38000 Grenoble, France

³Institute for Solid State and Materials Physics, Dresden University of Technology, 01062 Dresden, Germany

⁴Laboratoire National des Champs Magnétiques Intenses (LNCMI-EMFL),

CNRS, Université Grenoble Alpes, 38042 Grenoble, France

⁵Université Grenoble Alpes, CNRS, Institut Néel, 38000 Grenoble, France

⁶Institute for Quantum Materials and Technologies, Karlsruhe Institute of Technology, Kaiserstraße 12, 76131 Karlsruhe, Germany

(Dated: January 16, 2026)

Unconventional superconductivity in Ce-based Kondo-lattice materials emerges almost exclusively in the vicinity of weak dipolar magnetic orders, while higher multipolar orders are only known to occur in a few Pr-based unconventional superconductors and possibly URu_2Si_2 . The multiphase superconductor CeRh_2As_2 appears to be a notable exception from this trend. Showing clear signatures of magnetism, this tetragonal system is suspected to host a concomitant quadrupolar order, which could be causing the strong enhancement of the ordering temperature when a magnetic field is applied perpendicular to the fourfold (c) axis of the lattice. In this work, we show that the field-temperature phase diagram of CeRh_2As_2 has a remarkable basal-plane anisotropy. This finding supports the scenario of coupled magnetic and multipolar ordering, which may have implications for the pairing mechanism of the superconductivity, and guides the development of the next iteration of theoretical models.

Introduction.—The Kondo-lattice system CeRh_2As_2 is a heavy-fermion superconductor that exhibits a very rare magnetic-field-induced transition between two distinct superconducting (SC) phases [1]. These phases were proposed to be states of the even and odd parity of the SC order parameter [2–5], earning the material a significant attention.

However, the multiphase superconductivity is not the only intriguing phenomenon of CeRh_2As_2 . In accordance with the established paradigm of unconventional superconductivity [6], the compound is located close to a pressure-induced quantum critical point of another ordered state, known as phase I [7–9], which is quite unusual in and of itself. At ambient pressure, phase I sets in at the critical temperature T_0 (see Fig. 1), which is highly sensitive to static crystalline defects and reaches 0.54 K in the cleanest samples obtained so far [10]. The T_0 phase transition has a definite magnetic character, confirmed by muon spin resonance and nuclear magnetic/quadrupole resonance studies, although the ordering vector and moment orientations currently remain unknown [11–14]. Measurements of inelastic neutron scattering showed a very weak intensity at the $(1/2, 1/2, 0)$ wave vector [15], but the same study could not detect any long-range magnetic order, placing an upper limit of the ordered moment at 0.2 of Bohr magneton.

CeRh_2As_2 crystallises in a tetragonal non-symmorphic CaBe_2Ge_2 -type structure (space group 129, $P4/nmm$) [16], shown in Fig. 2. When a magnetic field $\mu_0 H$ (where μ_0 is the vacuum permeability) is applied along the c axis of the tetragonal unit cell, phase I is suppressed similar to a typical anti-ferromagnetic (AFM) state and vanishes at about 7 T [8, 10]. However, despite all the facts presented above, phase I cannot be understood as a conventional AFM order because of

the unusual robustness of T_0 against magnetic fields applied parallel to the basal plane of the lattice [7, 17, 18]. Moreover, as can be seen in Fig. 1, upon exceeding a critical field $\mu_0 H_{\text{cr}} \lesssim 9$ T, CeRh_2As_2 undergoes a transition from phase I into phase II. The latter state is characterised by a strong continuous increase of T_0 with the field. A recent pulsed-field study reported a cascade of further phase transitions occurring past 20 T, with a dome of electronic order stabilised up to 3.5 K near 60 T [19].

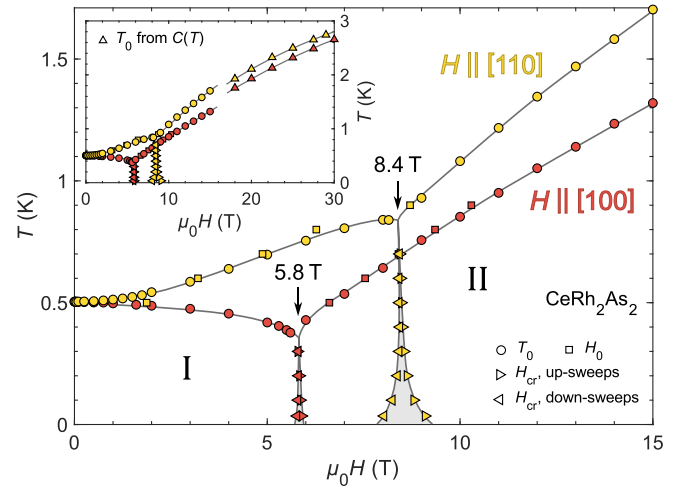


Figure 1. Phase diagrams of CeRh_2As_2 as functions of temperature (T) and magnetic field ($\mu_0 H$, where μ_0 is the vacuum permeability), applied along the [100] and [110] crystallographic directions. Phases I and II are indicated. The critical temperature (T_0) and fields (H_0 , H_{cr}) were extracted from measurements of T and H dependence of electrical resistivity, respectively. Solid grey lines are guides for the eye. The hysteretic regions are shaded in light-grey. The superconducting phase is omitted. Inset: an extension of the phase diagrams to higher fields according to heat capacity [$C(T)$] data.

* correspondence should be addressed to konstantin.semeniuk@cpfs.mpg.de and elena.hassinger@kit.edu

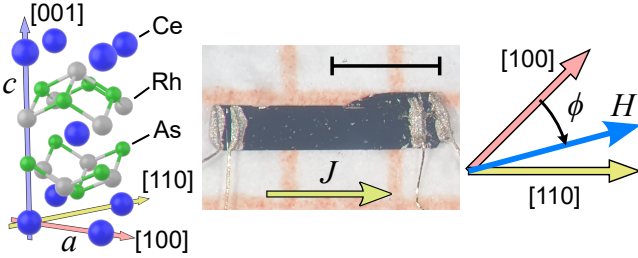


Figure 2. Left: tetragonal unit cell of CeRh_2As_2 . The crystallographic a and c axes as well as selected directions, labeled by Miller indices, are shown. Middle: photograph of the CeRh_2As_2 sample used for the resistivity measurements of this work. The yellow arrow indicates the direction of the current J . The scale bar marks a 1 mm distance. Right: orientation of the sample in the middle panel. In this study, a magnetic field H was applied perpendicular to the c axis, at a varied angle ϕ with respect to the [100] orientation.

Currently, the most promising explanation of the H - T phase diagram of CeRh_2As_2 for $H \perp c$ suggests that phases I and II (collectively called the T_0 order) involve a quadrupolar ordering, which occurs in tandem with a conventional AFM state [7, 20]. At a first glance, there is a caveat with such a scenario: for tetragonal Ce-based systems, the crystal-electric-field (CEF) scheme consists of three $J = 5/2$ Kramer's doublets, whereas quadrupolar orders, in contrast, require a four-fold degenerate CEF ground state and are therefore only known to exist in certain cubic Ce-based crystals, rather than tetragonal ones [21]. In CeRh_2As_2 , however, the first excited state was found to be only ~ 30 K above the ground state [22], and it has been shown theoretically that the two lowest-energy doublets can be mixed into a quasi-quartet by the Kondo coupling [7] and/or an in-plane (a axis) magnetic field [20], thus enabling a quadrupolar order. Its presence in phases I and II can be investigated by studying how $T_0(H)$ varies upon changing the field orientation within the basal-plane of the lattice. An anisotropic behaviour, together with the field-induced enhancement of T_0 , would support a quadrupolar or higher-order multipolar ordering. Given the details of this anisotropy one may be able to quantify the relative strength of different multipole components and couplings involved and refine information on the CEF scheme of CeRh_2As_2 .

In this letter, we show that the phase diagram of CeRh_2As_2 for $H \perp c$ has a significant basal-plane anisotropy, as depicted in Fig. 1. The enhancement of T_0 by the field was found to be stronger for $H \parallel [110]$ than for $H \parallel [100]$, along with a higher value of the critical field H_{cr} in the former case. The results cannot be readily captured by the existing model, motivating its extension as well as a re-examination of the CEF scheme of CeRh_2As_2 .

For our measurements, we used the latest generation of Bi-flux-grown CeRh_2As_2 crystals, which show a well-resolved and sharp heat capacity anomaly at T_0 [10]. We probed electrical resistivity (ρ), which shows clear signatures of the T_0 transition [7, 8]. The chosen sample was a thin elongated monocrystalline platelet with naturally formed extended flat facets normal to the c axis and straight edges along the [110]

direction and its equivalents, as determined via Laue X-ray diffraction (see Fig. 2 for the annotated photograph of the sample). For a 4-point resistivity measurement, gold wires were connected to the sample via spot-welding and were additionally reinforced with the DuPont 4922 silver paint. The electrical current was supplied and the voltage was probed along the [110] direction. The residual resistivity ratio (RRR) of the sample was $\rho(300\text{K})/\rho(0.5\text{K}) = 3.0$. The crystal was mounted on a rotating stage of a dilution refrigerator, with the c axis parallel to the rotation axis and perpendicular to the applied magnetic field. The uncertainty in the alignment was $\pm 2^\circ$. Measurements of heat capacity at high magnetic fields of up to 30 T were conducted at the EMFL facility in Grenoble, using an AC calorimetry method (see the Methods section of Ref. [23]) with a small, 0.12 mg crystal that ensured a good sample homogeneity.

Results.—We show the plots of $\rho(T)$ at fixed magnetic fields in Fig. 3a,b. The transition into phase I appears as an inflection of the curve, and we therefore used the minimum of $d\rho/dT$ as the definition of T_0 . Applying a magnetic field along the [100] direction (Fig. 3a) initially causes a weak decrease of T_0 . Between 5 and 6 T, the inflection of $\rho(T)$ is replaced by a downturn upon cooling, which is explained by phase II setting in instead of phase I. In the higher-field regime, we defined T_0 by the minimum of $d^2\rho/dT^2$ (the largest negative curvature). Above 6 T, T_0 steadily increases with the field reaching 1.3 K at 15 T and up to 2.7 K at 30 T (see the heat capacity data below).

Applying a field along the [110] direction (Fig. 3b) monotonically increases T_0 in the entire explored field range. The I-II transition occurs at a higher field, between 8 and 9 T. Above H_{cr} , T_0 increases with the field more rapidly than for $H \parallel [100]$, reaching 1.7 K (2.8 K) at 15 T (29 T).

In Fig. 3c,d, we plot $\rho(H)$ at fixed temperatures for the two field orientations. At lower temperatures, the I-II transition is clearly identified as a step-like decrease of resistivity upon increasing the field (we defined H_{cr} as the field at which the drop in $\rho(H)$ is the steepest). The first order character of the transition is apparent from the hysteresis. At temperatures high enough for the hysteresis to be negligible, H_{cr} is equal to 5.8 and 8.4 T for the [100] and [110] field directions, respectively.

We also used $\rho(H)$ curves for tracing the $T_0(H)$ line. Applying the same criteria as for T_0 (points of inflection and extremal curvature), we defined a critical field H_0 at which the system enters phases I and II (see Fig. 3c,d).

A few visible features in our data were likely caused by extrinsic effects. The small dip of $\rho(H)$ below 0.2 T indicates a presence of a small amount of an alien SC phase, possibly originating from the Bi flux. By extrapolating the $\rho(H)$ data down from above 0.2 T, we obtained the best estimates of $\rho(H=0)$ at the respective temperatures. The zero-field $\rho(T)$ curve shown in Fig. 3a,b has therefore been offset by a small positive value in order to correct for the influence of the alien phase. The existence of a surface state with the SC properties slightly different to those of the bulk may explain why the onset of the superconductivity in $\rho(H)$ for $H \parallel [110]$ has a double shoulder and is more gradual than for $H \parallel [100]$. The small differences between the upward and downward sweeps

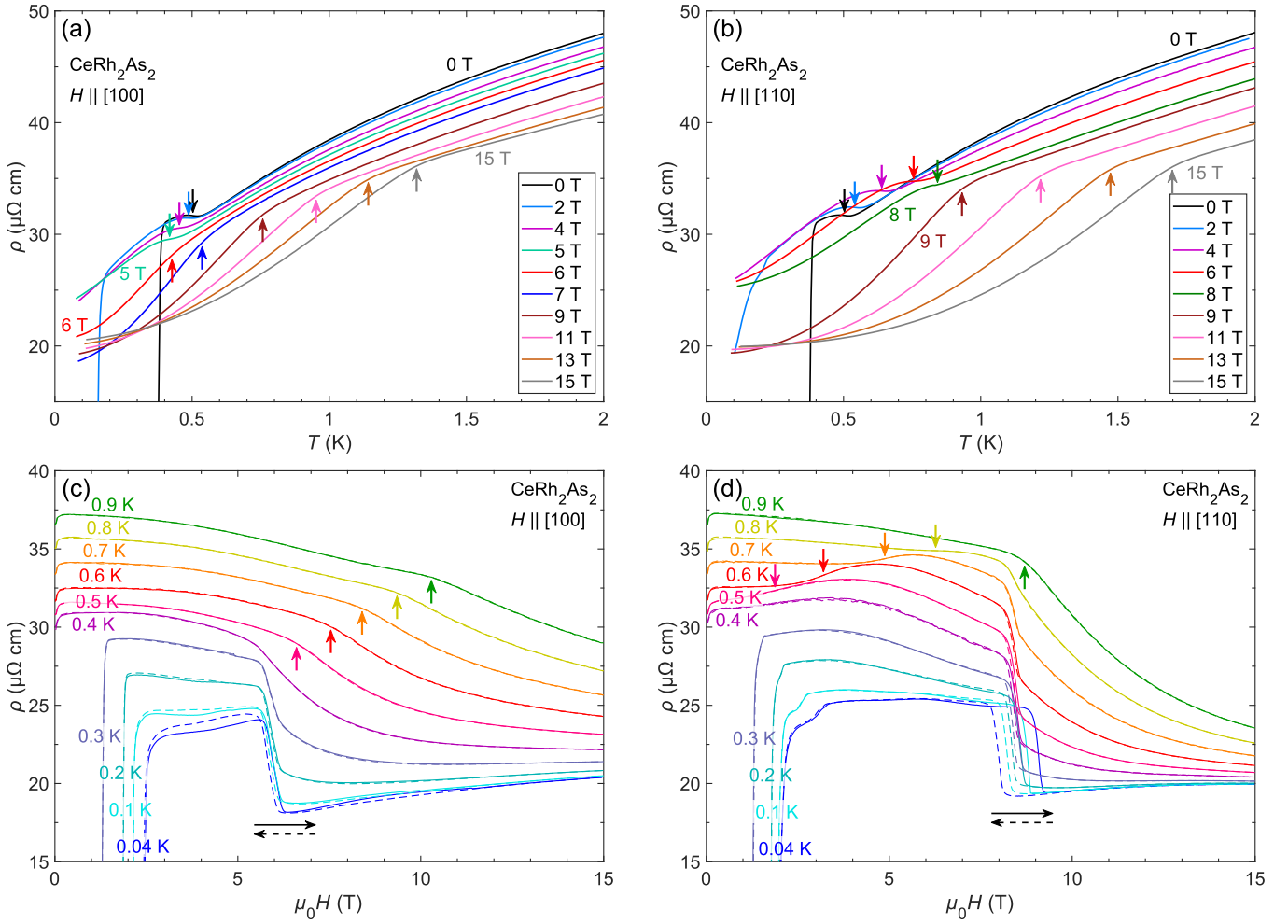


Figure 3. Electrical resistivity (ρ) of CeRh_2As_2 along the [110] crystallographic direction as a function of temperature T (a,b) and magnetic field $\mu_0 H$ (c,d) at fixed fields and temperatures, respectively. The field is applied along the [100] (a,c) and [110] (b,d) directions. The downward (upward) arrows mark the points of inflection (extremal curvature), defining the critical temperatures and fields of phase I (II) of CeRh_2As_2 .

of $\rho(H)$ below 0.3 K were likely caused by a slight temperature instability.

We supplement our resistivity study with high-field heat capacity data, shown in Fig. 4. The T_0 transition remains very pronounced up to 30 T, evidencing that the anomaly remains a phase transition and does not become a crossover. Applying the equal-entropy condition (see Supplemental Material below), we analysed how the height of the ideal heat capacity jump $\Delta C/T$ varies with the field (inset of Fig. 4b). For $H \parallel [100]$, $\Delta C/T$ stays approximately constant. For $H \parallel [110]$, while T_0 is higher, $\Delta C/T$ is smaller and decreases with the field.

Using the data above, we compiled the field-temperature phase diagrams for $H \parallel [100]$ and $H \parallel [110]$, shown in Fig. 1. The anisotropy of the T_0 order for fields within the basal plane is the strongest in Phase I, for which T_0 decreases with the [100]-oriented field, and increases with the [110]-oriented field. The high-field extensions of the phase boundaries based on the heat capacity data show a consistent anisotropy (Fig. 1 inset). The high-field portion of the data also reveals a gradual

flattening of the $T_0(H)$ line, in agreement with the dome-like shape observed in the pulsed-field study [19] and expected for a quadrupolar order [20].

We further probed T_0 for a range of magnetic field orientations between the [100] and [110] directions (Fig. 5a). The measurements were done with the field magnitudes fixed at 5.3 and 9.0 T, so that only phase I or phase II, respectively, could set in for all field orientations. In both cases, T_0 is at its maximum at $H \parallel [110]$ and decreases monotonically with a narrow minimum at $H \parallel [100]$. The relative anisotropy is visibly stronger for phase I ($A = T_0^{[110]}/T_0^{[100]} = 1.75$ at 5.3 T) compared to phase II ($A = 1.25$ at 9.0 T). The field-angle dependence of H_{cr} shows a similar picture (Fig. 5b). The narrower hysteresis for $H \parallel [100]$ can be attributed to a significantly smaller value of T_0 at H_{cr} .

Discussion.—Our observed basal-plane anisotropy of the T_0 order in CeRh_2As_2 explains the apparent discrepancy in the previously published phase diagrams for in-plane fields. The phase diagram for $H \parallel [100]$ in Ref. [18] agrees with our result, and namely with the decrease of T_0 with the field for

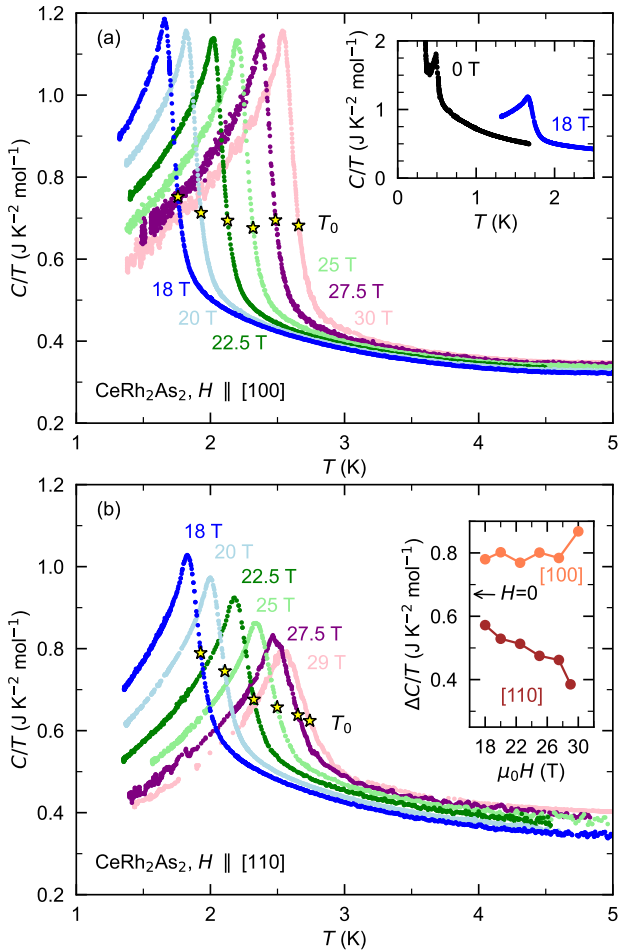


Figure 4. Heat capacity $C(T)$ of CeRh_2As_2 divided by temperature T at high magnetic fields applied along the [100] (a) and [110] (b) crystallographic directions. The yellow stars mark the critical temperatures T_0 of phase II, according to the equal entropy analysis. Panel (a) inset provides a comparison with $C(T)$ at zero field. The inset in panel (b) shows the corresponding heat capacity jump sizes $\Delta C/T$ at T_0 . The arrow marks the zero-field jump size

$\mu_0 H < \mu_0 H_{\text{cr}}^{[100]} = 5.8$ T. For the phase diagrams in Ref. [7] and Ref. [17], the field was pointing along the [110] direction or close to it, for which T_0 increases with the field both below and above $\mu_0 H_{\text{cr}}^{[110]} = 8.4$ T. The study in Ref. [7] found this value to be 9.0 T, but given the strong sensitivity of the T_0 order to static crystalline defects, and their possible influence on the hysteresis, such a difference between different generations of crystals is not too surprising.

The pronounced basal-plane magnetic anisotropy of phases I and II cannot be understood in terms of a dipolar order alone. For a tetragonal system like CeRh_2As_2 with the point group C_{4v} on the Ce site, the basal-plane components of the total magnetic dipole moment, J_x and J_y , belong to the same two-dimensional irreducible representation E (Γ_5 in Bethe notation). The only bilinear form they can take in the Hamiltonian, for it to remain invariant under a C_4 rotation, is

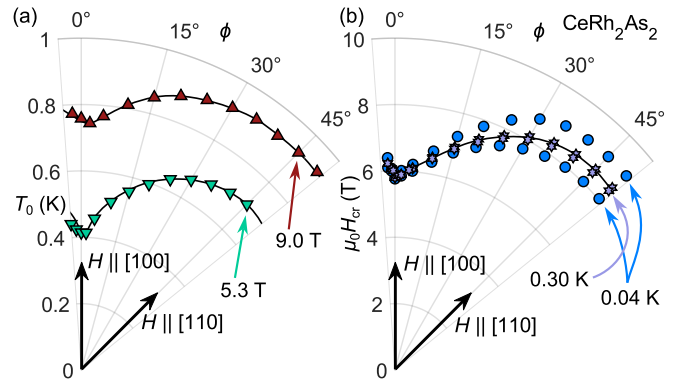


Figure 5. Magnetic-field-orientation dependence of the critical temperatures T_0 of phases I and II (a) and of the critical field H_{cr} of the I-II transition (b) in CeRh_2As_2 . The angle ϕ measures the basal-plane orientation of the field with respect to the [100] crystallographic direction. Measurements of T_0 were done at 5.3 and 9.0 T, when the system could only enter either phase I or phase II, respectively. The two values of H_{cr} plotted for each angle correspond to the transitions encountered in the upward and downward field sweeps. The solid black lines are guides to the eye. The data used for extracting the T_0 and H_{cr} values are provided in Supplemental Material.

$I_M(J_{i,x}J_{j,x} + J_{i,y}J_{j,y})$ (I_M is the coupling constant; i, j are the site indices). The exchange energy therefore depends on the relative orientation of the moments on two sites, rather than on the absolute ones, and a strictly dipolar order must respond to the in-plane field isotropically. For higher order multipoles, the moment components involved in the in-plane exchange generally do not belong to the same irreducible representation, making an anisotropic in-plane field response possible. This deduction is very much in line with the recent theoretical model that attempted to explain the unusual form of $T_0(H)$ for $H \parallel [100]$ with a field-induced antiferroquadrupolar (AFQ) order coupled to a conventional AFM order of the in-plane dipole [20].

The essential ingredient of the model is the structure of the CEF wave functions, which is also crucial for understanding the pronounced basal-plane anisotropy in CeRh_2As_2 . Two of the three Kramers doublets transform according to the same irreducible representation [20] and are therefore, in general, mixed, which is characterised by a (field-independent) mixing angle θ . In Ref. [20] it was shown for $H \parallel [100]$ that the physically relevant parameters are essentially given by $\xi_Q \propto m_{[100]}^2 I_Q$ where $m_{[100]} = m_{[100]}(\theta, H)$ is the field-induced intra-doublet matrix element and I_Q is the coupling of the O_{xy} component of the quadrupole. This results in a phase boundary given by the solid red curve in Fig. 6a, which captures the experimental findings surprisingly well, in a sense that it contains two regimes of distinguishable behaviour. At low fields, the AFM order parameter dominates over the AFQ one, and T_0 has a weaker field dependence. At higher fields, the dipolar order is suppressed, and the field-induced mixing of the first excited doublet into the CEF ground state generates and stabilises the AFQ order, causing the pronounced increase of T_0 . This outcome hints that phases I and II can be intuitively

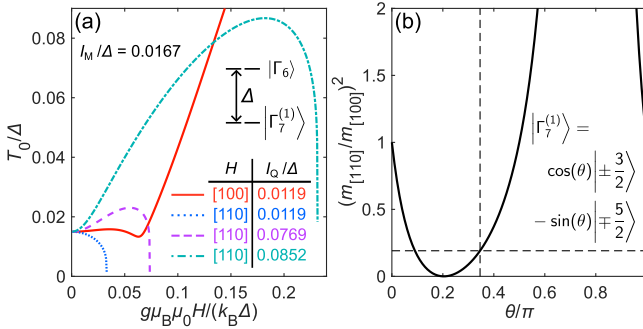


Figure 6. (a) Theoretical field (H) dependence of the critical temperature T_0 of CeRh_2As_2 , predicted by the magneto-quadrupolar ordering model [20]. The parameter Δ is the zero-field splitting between the two lowest-energy crystal-electric-field doublets $|\Gamma_7^{(1)}\rangle$ and $|\Gamma_6\rangle$; g , μ_B , μ_0 , and k_B are the electron g factor, Bohr magneton, vacuum permeability, and Boltzmann constant, respectively. The calculations were done for different orientations of H and different values of the quadrupolar exchange coupling I_Q (see the table). The in-plane isotropic magnetic exchange coupling I_M was kept fixed. (b) Squared ratio of the matrix elements of the relevant quadrupole components for the two field directions as a function of the mixing angle θ , which links the crystal-field states to the \hat{J}_z basis.

associated with a stronger and weaker role of the dipolar interaction, respectively (and vice versa for the quadrupolar interaction).

An obvious shortcoming of the model is its prediction of fundamentally the same ordered state in the entire domain of $T_0(H)$, while the experiment shows that phases I and II are distinct competing orders. Realising the first order transition at H_{cr} clearly requires a more complex description, including, for instance, magnetoelastic coupling or the Kondo effect. The fact that CeRh_2As_2 is a metal is strongly suggestive of a density wave picture of the T_0 order [7]. The distinct forms of the resistivity anomalies of phases I and II could reflect different Fermi surface reconstructions, with the H_{cr} transition corresponding to a change of the nesting vector. However, given that the electronic structure of the compound is inevitably linked to the crystal-field environment of the Ce site, it is not unexpected that a description based purely on local properties of f electrons can provide insights into the physics of the system (see Ref. [24], for instance).

It is natural to extend the model to the $H \parallel [110]$ case. The field then induces matrix elements $m_{[110]} = m_{[110]}(\theta, H)$ within the ground-state doublet of the $O_{x^2-y^2}$ quadrupole component, in a similar manner as for O_{xy} in the $H \parallel [100]$ case, but with a very different θ dependence. The results are summarised in Fig. 6: panel (a) shows the T_0 phase boundaries for $H \parallel [110]$ for three different choices of the AFQ coupling $I_Q(O_{x^2-y^2})$. The dotted blue curve corresponds to $I_Q(O_{x^2-y^2}) = I_Q(O_{xy})$, for the dashed purple and dash-dot teal curves we chose $I_Q(O_{x^2-y^2}) \gg I_Q(O_{xy})$. All other parameters, namely the mixing angle θ , the splitting Δ of the two low-lying doublets, and the isotropic in-plane AFM exchange I_M are the same as in Ref. [20]. For $I_Q(O_{x^2-y^2}) = I_Q(O_{xy})$, the T_0 order shows no field-induced enhancement for $H \parallel [110]$

and is strongly suppressed compared to the $H \parallel [100]$ case. This theoretical result is in stark contrast with our experimental findings, which can be attributed to two likely causes:

1. The matrix elements $m_{[110]}$ of the $O_{x^2-y^2}$ quadrupole component are strongly suppressed compared to $m_{[100]}$ for the O_{xy} component. For fields $h \ll \Delta$ this is illustrated in Fig. 6b where the vertical dashed line marks the mixing angle taken from Ref. [7], and the horizontal dashed line indicates the corresponding ratio $(m_{[110]}/m_{[100]})^2 \approx 0.29$. As seen in Fig. 6a, the influence of the matrix elements can be at least partially “compensated” by increasing the quadrupolar coupling strength $I_Q(O_{x^2-y^2})$. Note, that in the somewhat artificial case $\theta = 0$ (no mixing), $(m_{[110]}/m_{[100]})^2 = 1$, and the phase diagram is fully isotropic with respect to the basal-plane field direction.

2. The in-plane quadrupolar components O_{xy} and $O_{x^2-y^2}$ transform according to different irreducible representations, unlike the in-plane dipole components. Thus, there is no a priori reason why the combined AFM+AFQ phase boundary should be identical or even similar for different field directions. This is also reflected in the structure of the field-induced matrices of O_{xy} and $O_{x^2-y^2}$. The former contains pseudo-van-Vleck intra-doublet elements [20] while the latter contains pseudo-Curie type intra-doublet elements (see Supplemental Material below).

The comparison of the model with the experimentally observed basal-plane anisotropy of $T_0(H)$, and particularly the phase diagram for $H \parallel [110]$, suggests that a modification to the currently assumed CEF scheme of CeRh_2As_2 is necessary in order to better capture the phenomenology of the system.

Conclusions.—In this work, we exposed the pronounced magnetic basal-plane anisotropy of the ordered states of CeRh_2As_2 , known as phases I and II. The contrast between the fields along the $[100]$ and $[110]$ crystallographic directions is particularly strong for phase I, with the critical temperature T_0 decreasing and increasing with the field, respectively. This result supports the idea of the T_0 transition involving quadrupolar (or even higher-order multipolar) degrees of freedom, setting CeRh_2As_2 apart from all other Ce-based tetragonal heavy-fermion systems.

ACKNOWLEDGMENTS

We thank P. Thalmeier, G. Knebel, A. Pourret, S. Ruet, M. Brando, and G. Zwicknagl for fruitful discussions. The work was supported by the Deutsche Forschungsgemeinschaft (DFG) through CRC1143 (Project No. 247310070), the Würzburg-Dresden Cluster of Excellence on Complexity and Topology in Quantum Matter—ct.qmat (EXC 2147, Project ID 390858490), and the European Research Council (ERC) grant Ixtreme, GA 101125759. The authors also acknowledge the support of the LNCMI-CNRS, a member of the European Magnetic Field Laboratory (EMFL).

Supplemental Material

I. DETERMINATION OF T_0 FROM THE HEAT CAPACITY DATA VIA THE EQUAL-ENTROPY ANALYSIS

Fig. S1 illustrates the method for determining the critical temperature T_0 from the heat capacity data (Fig. 3 of the main paper), using the equal entropy construction. For an ideal heat capacity anomaly, the critical temperature of a second-order phase transition corresponds to the point where C changes discontinuously. In reality, various inhomogeneities throughout the sample broaden the anomaly, but it is sensible to assume that if we compare two temperatures, clearly below and above the range spanned by the anomaly, then the change in entropy between these two temperatures (area bounded by $C(T)/T$) is effectively the same as for an ideal crystal, since they correspond to the sample being completely in the ordered and disordered state, respectively. In order to determine T_0 , one needs to extrapolate the $C(T)/T$ curve for the ordered and unordered states towards the transition, and find such a position for the jump between them, that results in both the ideal and experimental curves resulting in the same entropy change across the anomaly.

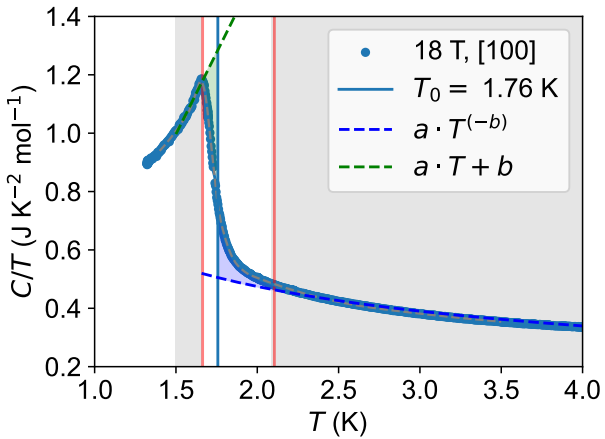


Figure S1. Illustration of the equal entropy method for determining the critical temperature T_0 of CeRh_2As_2 using the temperature (T) dependence of heat capacity divided by temperature (C/T). The example uses the data for 18 T magnetic field in the [100] direction (blue markers). The broadened heat capacity anomaly at the second-order phase transition is bounded by the two vertical red lines. Part of the curve located in the grey-shaded above (below) the anomaly is extrapolated across the anomaly using a power-law (linear) function. The extrapolations are shown in dashed lines and are supposed to reflect the behaviour of C/T in the ordered and unordered states for an ideal crystal. The parameters a and b are distinct for each extrapolation. The value of T_0 (blue vertical line) is chosen such that the area shaded in green is matched by the area shaded in blue.

II. RESISTIVITY DATA FOR THE ANGULAR DEPENDENCES OF T_0 AND H_{cr}

In Fig. S2 and Fig. S3, we show the field and temperature sweeps of resistivity for the field applied at different angles in the basal plane. These data provided the values of T_0 and H_{cr} for the polar plots in Fig. 5 of the main paper.

In the plots of $\rho(T)$ in the insets of Fig. S2, one can see that above T_0 all the curves collapse onto the same line, and the basal plane anisotropy develops only below T_0 . For the $\rho(H)$ plots, resistivity appears to be rather isotropic in Phase II at 0.04 K (Fig. S3a inset), but at 0.3 K resistivity varies with the angle both below and above H_{cr} (Fig. S3b inset).

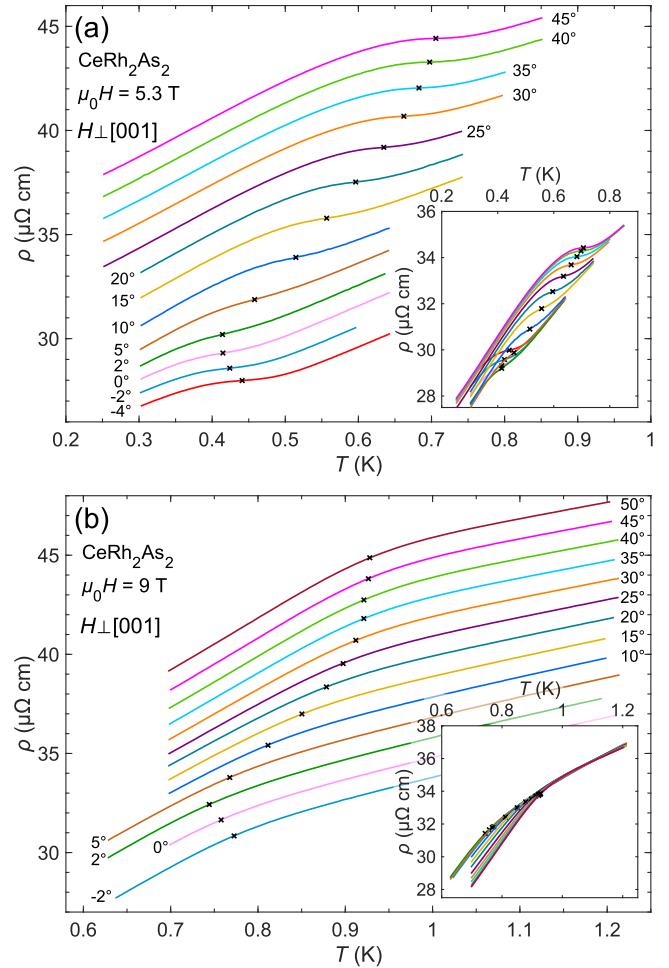


Figure S2. Electrical resistivity (ρ) of CeRh_2As_2 as a function of temperature (T) near the critical temperature T_0 (black crosses), for a magnetic field (H) applied along different directions in the basal plane. The angle of 0° corresponds to the field along the [100] crystallographic orientation. Resistivity was probed with the current flowing along the [110] direction. The magnitude of the field was set to 5.3 T (a) and 9.0 T (b), such that the system only enters Phase I or Phase II, respectively. The curves are offset in steps of $1 \mu\Omega \text{ cm}$, with respect to the 0° curve. The insets show the same data without the offsets.

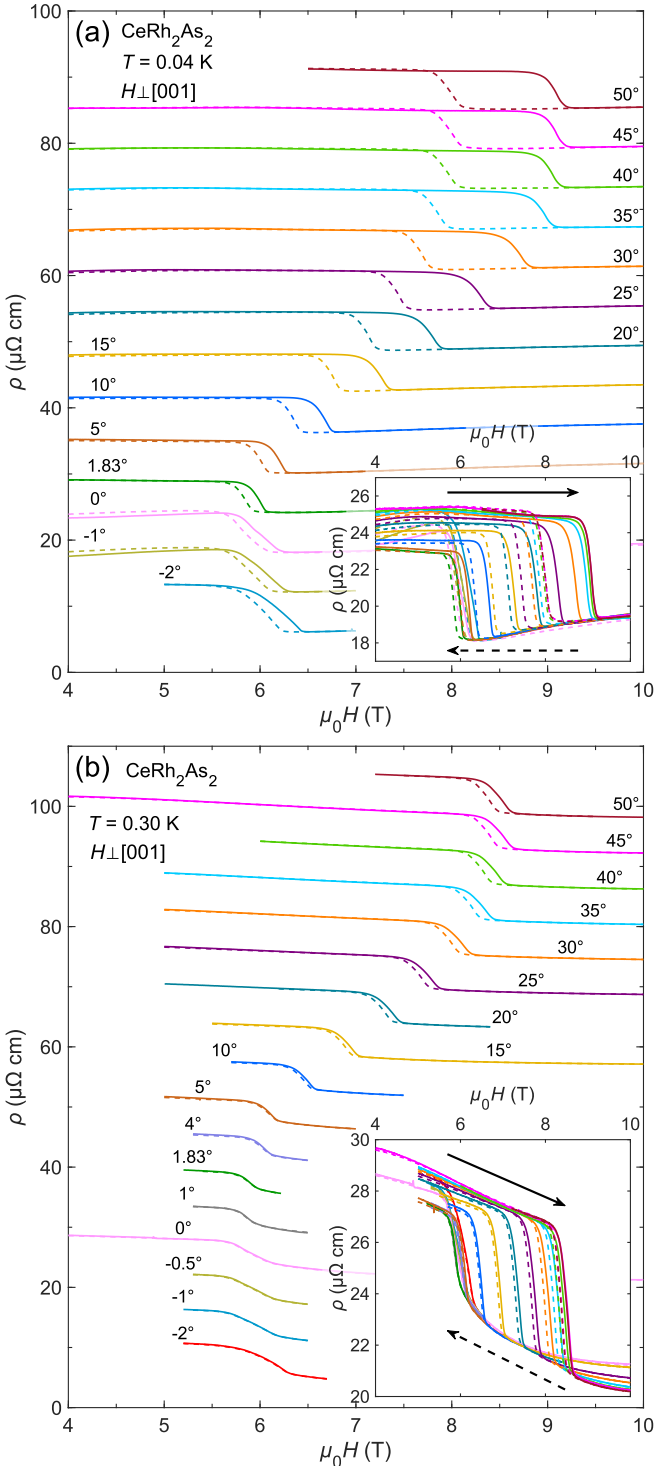


Figure S3. Electrical resistivity (ρ) of CeRh_2As_2 as a function of magnetic field (H) across the critical field H_{cr} of the Phase I-Phase II transition. The field was applied along different directions in the basal plane. The angle of 0° corresponds to the field along the $[100]$ crystallographic orientation. Resistivity was probed with the current flowing along the $[110]$ direction. The data were collected at different temperatures (T): 0.04 K (a) and 0.30 K (b). The curves are offset in steps of $6\text{ }\mu\Omega\text{ cm}$, with respect to the 0° curve. The insets show the same data without the offsets.

III. THE $O_{x^2-y^2}$ QUADRUPOLE COMPONENT

A. The single-ion Hamiltonian

In this section, we closely follow the derivations given in Ref. [20]. Now we assume the applied magnetic field to be oriented in the $[110]$ direction. First of all, let's diagonalise the single-ion Hamiltonian

$$\mathcal{H} = H_{\text{CEF}} + H_{\text{Zeeman}}, \quad (\text{S1})$$

$$H_{\text{CEF}} = B_2^0 O_2^0 + B_4^0 O_4^0 + B_4^4 O_4^4, \quad (\text{S2})$$

$$H_{\text{Zeeman}} = -g_j \mu_B \mu_0 H \frac{1}{\sqrt{2}} (J_x + J_y) =: -h J_{xy}. \quad (\text{S3})$$

Here, h is the sum of the external field H_0 and the induced molecular field along $[110]$. The spectrum of H_{CEF} is comprised of three Kramers doublets, the two low-lying of which form a quasi-quartet which we discuss from now on. We apply to it a series of unitary transformations, namely first an intra-doublet state transformation and then an inter-doublet state rotation, the latter characterised by two angles α_j , $j = 1, 2$. Bringing \mathcal{H} into diagonal form then requires

$$\tan(2\alpha_j) = (-)^j \frac{2h m'_a}{-\Delta + (-)^j h(m_{a_1} - m_{a_2})} \quad (\text{S4})$$

$$\Rightarrow \alpha_j \approx (-)^j \frac{h m'_a}{\Delta}, \quad \frac{h}{\Delta} \ll 1 \quad (\text{S5})$$

with $\hat{j} := 3 - j$ and $\alpha_j \neq \pi/4 + n\pi$, $n \in \mathbb{Z}$. The constants in Eq. (S4) are

$$\begin{aligned} m_{a_1} &:= -\frac{\sqrt{5}}{2} \sin(2\theta), \\ m_{a_2} &:= \frac{3}{2}, \\ m'_a &:= -\sqrt{2} \sin(\theta) \end{aligned}$$

with θ being the crystal-field mixing angle related to the crystal-field parameters like

$$\tan(2\theta) = \frac{-2\sqrt{5}B_4^4}{B_2^0 + 20B_4^0} \quad (\text{S6})$$

and $\theta \neq \pi/4 + n\pi$, $n \in \mathbb{Z}$.

B. The quadrupole component

The $H = 0$ bare quadrupole operator expressed in terms of the crystal-field (CEF) basis states has the form

$$O_{x^2-y^2}(\theta) = \left(\begin{array}{cccc|cc} 0 & 0 & m'_{Q_3} & 0 & 0 & 0 \\ 0 & 0 & 0 & m'_{Q_3} & 0 & 0 \\ m'_{Q_3} & 0 & 0 & 0 & m'_{Q_4} & 0 \\ 0 & m'_{Q_3} & 0 & 0 & 0 & m'_{Q_4} \\ \hline 0 & 0 & m'_{Q_4} & 0 & 0 & 0 \\ 0 & 0 & 0 & m'_{Q_4} & 0 & 0 \end{array} \right) \quad (\text{S7})$$

where the first four rows and columns denote the quasi-quartet. The matrix elements are given by

$$\begin{aligned} m'_{Q_3} &:= \sqrt{2} \left(\sqrt{5} \cos(\theta) - 3 \sin(\theta) \right), \\ m'_{Q_4} &:= \sqrt{2} \left(3 \cos(\theta) + \sqrt{5} \sin(\theta) \right). \end{aligned}$$

Applying the same unitary transformations which bring the Hamiltonian (S1) restricted to the quasi-quartet into diagonal

form, we eventually obtain

$$O_{x^2-y^2} \rightarrow \begin{pmatrix} -\tilde{M}_{Q_3}^{1s} & 0 & \tilde{M}_{Q_3}^{1c} & 0 \\ 0 & -\tilde{M}_{Q_3}^{2s} & 0 & \tilde{M}_{Q_3}^{2c} \\ \tilde{M}_{Q_3}^{1c} & 0 & \tilde{M}_{Q_3}^{1s} & 0 \\ 0 & \tilde{M}_{Q_3}^{2c} & 0 & \tilde{M}_{Q_3}^{2s} \end{pmatrix}. \quad (\text{S8})$$

with field-induced ($\alpha_j \neq 0$) matrix elements

$$\tilde{M}_{Q_3}^{j\eta} := m'_{Q_3} \begin{cases} \sin(2\alpha_j), & \eta = s \\ \cos(2\alpha_j), & \eta = c \end{cases} \quad (\text{S9})$$

depending both on field and CEF mixing angle. We stress that only for field $h \neq 0$ we obtain finite intra-doublet matrix elements $\tilde{M}_{Q_3}^{js} \neq 0$. In the main text, we use the notation $m_{[110]} = |\tilde{M}_{Q_3}^{js}|$.

[1] S. Khim, J. F. Landaeta, J. Banda, N. Bannor, M. Brando, P. M. R. Brydon, D. Hafner, R. Küchler, R. Cardoso-Gil, U. Stockert, A. P. Mackenzie, D. F. Agterberg, C. Geibel, and E. Hassinger, Field-induced transition within the superconducting state of CeRh_2As_2 , *Science* **373**, 1012 (2021).

[2] J. F. Landaeta, P. Khanenko, D. C. Cavanagh, C. Geibel, S. Khim, S. Mishra, I. Sheikin, P. M. R. Brydon, D. F. Agterberg, M. Brando, and E. Hassinger, Field-Angle Dependence Reveals Odd-Parity Superconductivity in CeRh_2As_2 , *Phys. Rev. X* **12**, 031001 (2022).

[3] T. Yoshida, M. Sigrist, and Y. Yanase, Pair-density wave states through spin-orbit coupling in multilayer superconductors, *Phys. Rev. B* **86**, 134514 (2012).

[4] T. Yoshida, M. Sigrist, and Y. Yanase, Parity-mixed superconductivity in locally non-centrosymmetric system, *J. Phys. Soc. Japan* **83**, 013703 (2014).

[5] M. H. Fischer, M. Sigrist, D. F. Agterberg, and Y. Yanase, Superconductivity and Local Inversion-Symmetry Breaking, *Annu. Rev. Condens. Matter Phys.* **14**, 153 (2023).

[6] N. D. Mathur, F. M. Grosche, S. R. Julian, I. R. Walker, D. M. Freye, R. K. W. Haselwimmer, and G. G. Lonzarich, Magnetically mediated superconductivity in heavy fermion compounds, *Nature* **394**, 39 (1998).

[7] D. Hafner, P. Khanenko, E.-O. Eljaouhari, R. Küchler, J. Banda, N. Bannor, T. Lühmann, J. F. Landaeta, S. Mishra, I. Sheikin, E. Hassinger, S. Khim, C. Geibel, G. Zwicknagl, and M. Brando, Possible Quadrupole Density Wave in the Superconducting Kondo Lattice CeRh_2As_2 , *Phys. Rev. X* **12**, 011023 (2022).

[8] K. Semeniuk, D. Hafner, P. Khanenko, T. Lühmann, J. Banda, J. F. Landaeta, C. Geibel, S. Khim, E. Hassinger, and M. Brando, Decoupling multiphase superconductivity from normal state ordering in CeRh_2As_2 , *Phys. Rev. B* **107**, L220504 (2023).

[9] M. Pfeiffer, K. Semeniuk, J. F. Landaeta, R. Borth, C. Geibel, M. Nicklas, M. Brando, S. Khim, and E. Hassinger, Pressure-tuned quantum criticality in the locally noncentrosymmetric superconductor CeRh_2As_2 , *Phys. Rev. Lett.* **133**, 126506 (2024).

[10] P. Khanenko, J. F. Landaeta, S. Ruet, T. Lühmann, K. Semeniuk, M. Pelly, A. W. Rost, G. Chajewski, D. Kaczorowski, C. Geibel, S. Khim, E. Hassinger, and M. Brando, Phase diagram of CeRh_2As_2 for out-of-plane magnetic field, *Phys. Rev. B* **112**, L060501 (2025).

[11] S. Khim, O. Stockert, M. Brando, C. Geibel, C. Baines, T. J. Hicken, H. Luetkens, D. Das, T. Shiroka, Z. Guguchia, and R. Scheuermann, Coexistence of local magnetism and superconductivity in the heavy-fermion compound CeRh_2As_2 revealed by μSR studies, *Phys. Rev. B* **111**, 115134 (2025).

[12] S. Kitagawa, M. Kibune, K. Kinjo, M. Manago, T. Taniguchi, K. Ishida, M. Brando, E. Hassinger, C. Geibel, and S. Khim, Two-Dimensional XY-Type Magnetic Properties of Locally Noncentrosymmetric Superconductor CeRh_2As_2 , *J. Phys. Soc. Japan* **91**, 043702 (2022).

[13] M. Kibune, S. Kitagawa, K. Kinjo, S. Ogata, M. Manago, T. Taniguchi, K. Ishida, M. Brando, E. Hassinger, H. Rosner, C. Geibel, and S. Khim, Observation of Antiferromagnetic Order as Odd-Parity Multipoles inside the Superconducting Phase in CeRh_2As_2 , *Phys. Rev. Lett.* **128**, 057002 (2022).

[14] S. Ogata, S. Kitagawa, K. Kinjo, K. Ishida, M. Brando, E. Hassinger, C. Geibel, and S. Khim, Parity Transition of Spin-Singlet Superconductivity Using Sublattice Degrees of Freedom, *Phys. Rev. Lett.* **130**, 166001 (2023).

[15] T. Chen, H. Siddiquee, Q. Xu, Z. Rehfuss, S. Gao, C. Lygouras, J. Drouin, V. Morano, K. E. Avers, C. J. Schmitt, A. Podlesnyak, J. Paglione, S. Ran, Y. Song, and C. Broholm, Quasi-two-dimensional antiferromagnetic spin fluctuations in the spin-triplet superconductor candidate CeRh_2As_2 , *Phys. Rev. Lett.* **133**, 266505 (2024).

[16] R. Madar, P. Chaudouet, J. Senateur, S. Zemni, and D. Tranqui, New ternary pnictides with the CaBe_2Ge_2 -type structure in the systems, rare-earth-Rh-P and rare-earth-Rh-As, *J. less-common met.* **133**, 303 (1987).

[17] S. Mishra, Y. Liu, E. D. Bauer, F. Ronning, and S. M. Thomas, Anisotropic magnetotransport properties of the heavy-fermion superconductor CeRh_2As_2 , *Phys. Rev. B* **106**, L140502 (2022).

[18] G. Chajewski and D. Kaczorowski, Discovery of magnetic phase transitions in heavy-fermion superconductor CeRh_2As_2 , *Phys. Rev. Lett.* **132**, 076504 (2024).

[19] J. Bławat, G. Chajewski, D. Gnida, J. Singleton, O. Ayala Valenzuela, D. Kaczorowski, and R. D. McDonald, Competing Electronic Ground States in the Heavy-Fermion Superconductor CeRh_2As_2 , *Phys. Rev. X* **15**, 041057 (2025).

- [20] B. Schmidt and P. Thalmeier, Anisotropic magnetic and quadrupolar H – T phase diagram of CeRh_2As_2 , *Phys. Rev. B* **110**, 075154 (2024).
- [21] K. Hanzawa and T. Kasuya, Antiferro-Quadrupolar ordering in CeB_6 , *J. Phys. Soc. Japan* **53**, 1809 (1984).
- [22] D. S. Christovam, M. Ferreira-Carvalho, A. Marino, M. Sundermann, D. Takegami, A. Melendez-Sans, K. D. Tsuei, Z. Hu, S. Rößler, M. Valvidares, M. W. Haverkort, Y. Liu, E. D. Bauer, L. H. Tjeng, G. Zwicknagl, and A. Severing, Spectroscopic evidence of kondo-induced quasiquartet in CeRh_2As_2 , *Phys. Rev. Lett.* **132**, 046401 (2024).
- [23] Z. Yang, C. Marcenat, S. Kim, S. Imajo, M. Kimata, T. Nomura, A. De Muer, D. K. Maude, F. Iga, T. Klein, D. Chowdhury, and Y. Kohama, Evidence for large thermodynamic signatures of in-gap fermionic quasiparticle states in a kondo insulator, *Nat. Commun.* **15**, 7801 (2024).
- [24] P. Thalmeier, A. Akbari, and R. Shiina, Multipolar order and excitations in rare-earth boride kondo systems, in *Rare-Earth Borides*, edited by D. S. Inosov (Jenny Stanford Publishing, Singapore, 2022) Chap. 8.